Generating higher-order quantum dissipation from lower-order parametric processes

2017 Quantum Sci. Technol. 2 024005

(http://iopscience.iop.org/2058-9565/2/2/024005)

Quantum Science and Technology

RECEIVED
16 February 2017

REVISED
14 April 2017

ACCEPTED FOR PUBLICATION
21 April 2017

PUBLISHED
24 May 2017

PAPER

Generating higher-order quantum dissipation from lower-order parametric processes

S O Mundhada[1,4], A Grimm[1], S Touzard[1], U Vool[1], S Shankar[1], M H Devoret[1] and M Mirrahimi[2,3]

[1] Department of Applied Physics, Yale University, New Haven, Connecticut 06520, United States of America
[2] QUANTIC team, INRIA de Paris, 2 Rue Simone Iff, F-75012 Paris, France
[3] Yale Quantum Institute, Yale University, New Haven, Connecticut 06520, United States of America
[4] Author to whom any correspondence should be addressed.

E-mail: shantanu.mundhada@yale.edu

Keywords: quantum information, dissipation engineering, quantum error correction, superconducting quantum computation

Abstract

The stabilisation of quantum manifolds is at the heart of error-protected quantum information storage and manipulation. Nonlinear driven-dissipative processes achieve such stabilisation in a hardware efficient manner. Josephson circuits with parametric pump drives implement these nonlinear interactions. In this article, we propose a scheme to engineer a four-photon drive and dissipation on a harmonic oscillator by cascading experimentally demonstrated two-photon processes. This would stabilise a four-dimensional degenerate manifold in a superconducting resonator. We analyse the performance of the scheme using numerical simulations of a realisable system with experimentally achievable parameters.

1. Introduction

To achieve a robust encoding and processing of quantum information, it is important to stabilise not only individual quantum states, but the entire manifold spanned by their superpositions to create a decoherence free subspace [1–5]. This requires synthesising artificial interactions with desirable properties which are impossible to find in natural systems. Particularly, in the case of quantum superconducting circuits, Josephson junctions together with parametric pumping methods provide powerful hardware elements for the design of such Hamiltonians. Here we extend the design toolkit, by using ideas borrowed from Raman processes to achieve Hamiltonians of high-order nonlinearity. More precisely, we introduce a novel nonlinear driven-dissipative process stabilising a four-dimensional degenerate manifold.

In general, a quantum system interacting with its environment will decohere through the entanglement between the environmental and the system degrees of freedom. However, in certain cases, a driven system with a properly tailored interaction with an environment can remain in a pure excited state or even a manifold of excited states [6–19]. The simplest example is a driven harmonic oscillator with an ordinary dissipation, i.e. a frictional force proportional to velocity. In the underdamped quantum regime, this friction corresponds to the harmonic oscillator undergoing a single-photon loss process. Such a driven-dissipative process, in the rotating frame of the harmonic oscillator, can be modelled by the master equation

$$\frac{\mathrm{d}}{\mathrm{d}t}\rho = -i[\epsilon_d \hat{a}^\dagger + \epsilon_d^* \hat{a},\ \rho] + \kappa \mathcal{D}[\hat{a}]\rho,$$

where ρ is the density operator, $\hat{a}$ is the harmonic oscillator annihilation operator, ϵ_d represents the resonant complex amplitude of the resonant drive, κ is the dissipation rate of the harmonic oscillator and

$$\mathcal{D}[\hat{L}]\rho = \hat{L}\rho\hat{L}^\dagger - \frac{1}{2}\hat{L}^\dagger\hat{L}\rho - \frac{1}{2}\rho\hat{L}^\dagger\hat{L}$$

is the Lindblad super-operator. The system admits a pure steady state, which is a coherent state denoted by $|\alpha\rangle$ where $\alpha = -2i\epsilon_d/\kappa$. Note also that the right-hand side of the above master equation can be simply written as $\kappa\mathcal{D}[\hat{a} - \alpha]\rho$. The fact that $|\alpha\rangle$ is the steady state of the process follows from $(\hat{a} - \alpha)|\alpha\rangle = 0$. This idea can be

generalised to a nonlinear dissipation of the form $\kappa\mathcal{D}[a^n - \alpha^n]\rho$ which admits as steady states the n coherent states $\{|\alpha e^{2im\pi/n}\rangle\}_{m=0}^{n-1}$. Indeed, all these coherent states and their superpositions are in the kernel of the dissipation operator $(a^n - \alpha^n)$. Therefore, this process stabilises the whole n-dimensional manifold spanned by the above coherent states.

The case with $n = 2$ has been proposed in [20–24] and experimentally realised in [25]. The idea consists of mediating a coupling between a high-Q cavity mode (resonance frequency ω_a) and a low-Q resonator (resonance frequency ω_b) through a Josephson junction. Applying a strong microwave drive at frequency $\omega_{\text{pump}} = 2\omega_a - \omega_b$ and a weaker drive at frequency ω_b, we achieve an effective interaction Hamiltonian of the form

$$\frac{H_{2\text{ph}}}{\hbar} = (g_{2\text{ph}}^{*}\hat{a}^{\dagger 2}\hat{b} + g_{2\text{ph}}\hat{a}^{2}\hat{b}^{\dagger}) - (\epsilon_d^{*}\hat{b} + \epsilon_d\hat{b}^{\dagger}).$$

Combining this interaction with a strong dissipation $\Gamma\mathcal{D}[\hat{b}]$ at the rate $\Gamma \gg |g_{2\text{ph}}|$ translates to an effective dissipation of the form $\kappa_{2\text{ph}}\mathcal{D}[\hat{a}^2 - \alpha^2]\rho$, where $\kappa_{2\text{ph}} = 4|g_{2\text{ph}}|^2/\Gamma$ and $\alpha = \sqrt{\epsilon_d/g_{2\text{ph}}}$. Here, we go beyond this by exploring a scheme which enables nonlinear dissipation of higher-order. More precisely, we propose a method to achieve a four-photon interaction Hamiltonian without significantly increasing the required hardware complexity. The idea consists of using a Raman-type process [26], exploiting virtual transitions, to cascade two $H_{2\text{ph}}$ interactions.

An important application of such a manifold stabilisation is error-protected quantum information encoding and processing. Specifically, Leghtas *et al* [27] have proposed employing four-component Schrödinger cat states

$$|\mathcal{C}_\alpha^{(k \bmod 4)}\rangle = \mathcal{N}(|\alpha\rangle + (-1)^k|\alpha\rangle + (i)^k|i\alpha\rangle + (-i)^k|i\alpha\rangle)$$

to encode quantum information that would be protected in a hardware efficient manner. Here $\mathcal{N}$ is a normalization constant. The states with $k = 0, 2$ have an even photon-number parity and $k = 1, 3$ have an odd parity. A photon loss error on the cavity changes the parity of the states as shown by

$$a|\mathcal{C}_\alpha^{(k \bmod 4)}\rangle / ||a|\mathcal{C}_\alpha^{(k \bmod 4)}\rangle|| = |\mathcal{C}_\alpha^{((k+1) \bmod 4)}\rangle.$$

Hence, by encoding the information in the even (or odd) sub-manifold of the cat states, we can monitor the photon loss error by measuring the photon-number parity as demonstrated in [28, 29]. In addition, protecting the information against both cavity dephasing and energy relaxation requires stabilising the four constituent coherent states simultaneously using a four-photon driven-dissipative process as shown by Mirrahimi *et al* [24]. The stabilisation is also a prerequisite for certain quantum operations [24, 30] and facilitates the realisation of a logical qubit.

With the goal of engineering a four-photon driven-dissipative process in mind, we first describe a scheme to achieve a four-photon exchange Hamiltonian in section 2. In section 3, we study the dynamics in presence of dissipation of the low-Q mode along with possible improvements. In appendices A and B, we discuss the derivation of the effective master equation and the accuracy of approximations used in the analytical calculations.

2. Cascading nonlinear processes

Similar to the ideas presented in the last section, to have four-photon dissipation, we need to build a process that exchanges four cavity photons with an excitation in a dissipative mode. Following the example of the two-photon process, this could be realised by engineering an interaction Hamiltonian of the form $H_{\text{int}}/\hbar = g_{4\text{ph}}\hat{a}^4\hat{b}^{\dagger} + g_{4\text{ph}}^{*}\hat{a}^{4\dagger}\hat{b}$ which is exchanging four photons of the cavity mode with a single excitation of the low-Q mode. We need the strength of the interaction $|g_{4\text{ph}}|$ to significantly exceed the decay rate of the storage cavity mode $\hat{a}$.

The Hamiltonian of a Josephson junction provides us with a six-wave mixing process, which combined with an off-resonant pump at frequency $\omega_p = 4\omega_a - \omega_b$ could, in principle, produce such an interaction. However, this six-wave mixing process comes along with other nonlinear terms in the Hamiltonian which could be of the same or higher magnitude. In particular, as it has been explained in [24], with the currently achievable experimental parameters, the cavity self-Kerr effect would be at least an order of magnitude larger than $|g_{4\text{ph}}|$.

A more elaborate Josephson circuit to realise a purer interaction Hamiltonian is proposed in [24]. This, however, comes at the expense of significant hardware development and might encounter other unknown experimental limitations. Here we propose an alternative approach, which is based on cascading two-photon exchange processes. This leads to significant hardware simplifications and could in principle be realised with current experimental setups [25]. In the next subsection, we give a schematic representation of the proposed protocol, which uses higher energy levels of the junction mode and a cascading based on Raman transition [26]. In section 2.2, we sketch a mathematical analysis based on the second-order rotating wave approximation

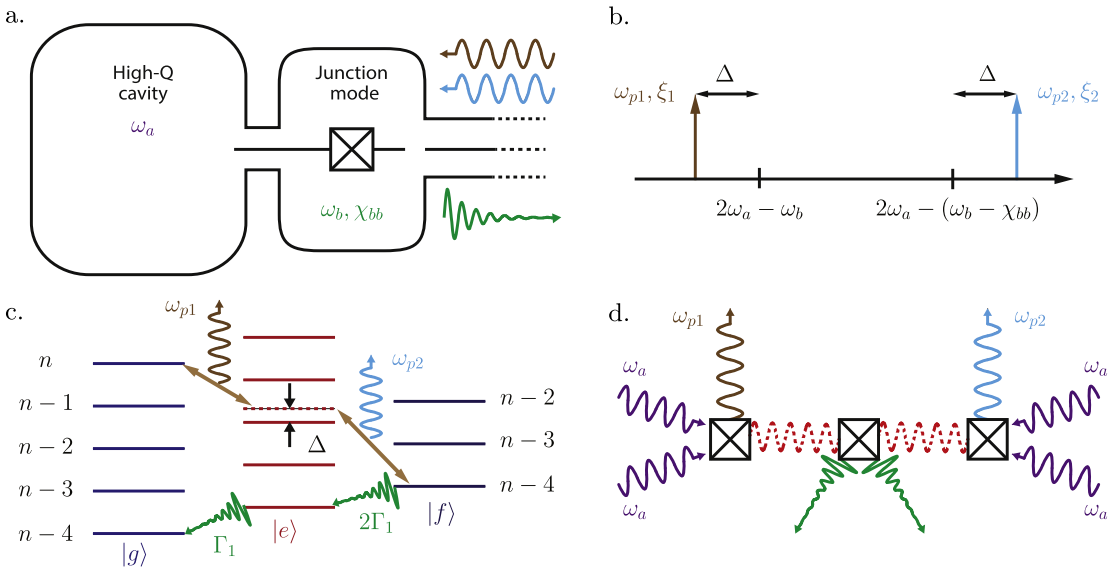

Figure 1. Basic principle behind cascading two-photon exchange processes. (a) A high-Q cavity at frequency ω_a coupled to a Josephson junction mode at frequency ω_b and anharmonicity χ_{bb}. The system can be driven through a transmission line coupled to the junction mode as shown. (b) Driving the system at frequency $2\omega_a - \omega_b$ ($2\omega_a - \omega_b + \chi_{bb}$) would lead to an exchange of two cavity photons with the $g - e$ ($e - f$) excitations of the junction mode. Instead, by detuning the drives by Δ (respectively $-\Delta$) only a cascade of two such exchanges is possible, leading to a four-photon exchange. (c) Explanation of the cascading process using the energy level description of the junction-cavity system. Here, the Fock-states of the cavity are denoted by numbers and the lowest three eigenstates of the junction mode are denoted by letters g, e and f. The first pump (brown) connects the state $|g, n\rangle$ with a virtual state detuned from state $|e, n-2\rangle$ by Δ (red dashed line). The second pump (cyan) connects this virtual state with the state $|n-4, f\rangle$. Thus a pair of two-photon exchanges are combined to create a four-photon transition from $|g, n\rangle$ to $|f, n-4\rangle$. (d) Diagramatic representation of the four-photon exchange process. Two pairs of cavity photons (purple) each combine with a pump photon to produce a virtual junction excitation (dashed red). The resulting two virtual excitations in turn combine to create two real junction photons (green).

(RWA). This is supplemented by numerical simulations comparing the exact and the approximate Hamiltonians.

2.1. Four-photon exchange scheme

To combine a pair of two-photon exchange processes, we take advantage of the junction mode being a multilevel anharmonic system. The basic principle of our scheme is illustrated in figure 1. More precisely, we exchange four cavity photons with two excitations of the junction mode. This could be done in a sequential manner by exchanging, twice, two cavity photons with an excitation of the junction mode, once from g to e and then from e to f. However, as will be seen later, populating the e level of the junction mode leads to undesired decoherence channels for the cavity mode. Therefore, we perform this cascading using a virtual transition through the e level by detuning the two-photon exchange pumps. This is similar to a Raman transition in a three level system.

Consequently, we apply two pumps at frequencies, $\omega_{p1} = 2\omega_a - \omega_b - \Delta$ and $\omega_{p2} = 2\omega_a - (\omega_b - \chi_{bb}) + \Delta$ as shown in figure 1(a). Note that here we are considering the $\hat{b}$ mode to be a junction mode with frequency ω_b and anharmonicity χ_{bb}. For this protocol to work, we require $\chi_{bb} \gg \Delta$, as we will justify in the next section. Starting in the state $|g, n\rangle$ these pumps make a transition to the state $|f, n-4\rangle$, passing virtually through the state $|e, n-2\rangle$ (see figure 1(b)). As will be seen in section 3, to achieve four-photon dissipation we also require the junction mode to dissipate from the f to the g state.

2.2. Analytical derivation using second-order RWA

Here, starting from the full Hamiltonian of the junction-cavity system, we provide a mathematical analysis of the proposed scheme. We also include an additional drive in our calculations, which will address a two-photon transition between the g and f levels of the junction mode. The importance of this drive will be clear in section 3 when we talk about a four-photon driven-dissipative process. The starting Hamiltonian is given by [31]

$$\frac{H(t)}{\hbar} = \omega_a \hat{a}^\dagger \hat{a} + \omega_b \hat{b}^\dagger \hat{b} - \frac{E_J}{\hbar}\left[\cos(\hat{\varphi}) + \frac{\hat{\varphi}^2}{2!}\right] + \sum_{k=0}^{3} \epsilon_{pk}(t)(\hat{b} + \hat{b}^\dagger),$$

where E_J is the Josephson energy and $\hat{\varphi} = \phi_a(\hat{a} + \hat{a}^\dagger) + \phi_b(\hat{b} + \hat{b}^\dagger)$. Here, $\phi_{a(b)} = \phi_{\mathrm{ZPF},a(b)}/\phi_0$ with $\phi_{\mathrm{ZPF},a(b)}$ corresponds to the zero point fluctuations of the two modes as seen by the junction and $\phi_0 = \hbar/2e$ is the reduced superconducting flux quantum. The drive fields $\epsilon_{pk}(t) = 2\epsilon_{pk}\cos(\omega_{pk}t + \theta_k)$ represent the off-

resonant pump terms The pump frequencies are selected to be

$$\begin{aligned}\omega_{p1} &= 2\tilde{\omega}_a - \tilde{\omega}_b - \Delta + \delta \\ \omega_{p2} &= 2\tilde{\omega}_a - (\tilde{\omega}_b - \chi_{bb}) + \Delta + \delta \\ \omega_{p3} &= \tilde{\omega}_b - \frac{\chi_{bb}}{2} - \frac{\delta}{2}\end{aligned} \tag{1}$$

where $\tilde{\omega}_a$ and $\tilde{\omega}_b$ are Lamb and Stark shifted cavity and junction mode frequencies. The additional detuning $\delta \ll \Delta$ will be selected to compensate for higher-order frequency shifts.

Following the supplementary material of [25], we go into a displaced frame absorbing the pump terms in the cosine. This leads to the Hamiltonian

$$\frac{H'(t)}{\hbar} = \omega_a \hat{a}^\dagger \hat{a} + \omega_b \hat{b}^\dagger \hat{b} - E_J \left[\cos(\hat{\Phi}(t)) + \frac{\hat{\Phi}^2(t)}{2!}\right],$$

where

$$\hat{\Phi}(t) = \phi_a \hat{a} + \phi_b \hat{b} + \phi_b \sum_{k=1}^{3} \xi_k \exp(-i\omega_{pk} t) + \text{h.c.}$$

Here, h.c. stands for Hermitian conjugate and ξ_k are complex coefficients related to phases and amplitudes of the pumps.

Developing the cosine up to fourth-order terms and keeping only the diagonal and the two-photon exchange terms, we get a Hamiltonian of the form

$$\begin{aligned}\frac{H_{\text{sys}}(t)}{\hbar} = {} & \tilde{\omega}_a \hat{a}^\dagger \hat{a} + \tilde{\omega}_b \hat{b}^\dagger \hat{b} - \frac{\chi_{aa}}{2} \hat{a}^{\dagger 2} \hat{a}^2 - \frac{\chi_{bb}}{2} \hat{b}^{\dagger 2} \hat{b}^2 - \chi_{ab} \hat{a}^\dagger \hat{a} \hat{b}^\dagger \hat{b} \\ & + \sum_{k=1,2} (g_k \exp(-i\omega_{pk} t)) \hat{a}^{\dagger 2} \hat{b} + \text{h.c.}) - (g_3 \exp(2i\omega_{p3} t)) \hat{b}^2 + \text{h.c.}).\end{aligned} \tag{2}$$

Here, we ignored all the other terms assuming a sufficiently large frequency difference, $|\tilde{\omega}_a - \tilde{\omega}_b|$, between the two modes. Indeed, in the rotating frame of $\tilde{\omega}_a \hat{a}^\dagger \hat{a} + \tilde{\omega}_b \hat{b}^\dagger \hat{b}$, these terms will be oscillating at significantly higher frequencies. In the above Hamiltonian, χ_{aa}, χ_{bb} and χ_{ab} are, respectively, the self-Kerr and cross-Kerr couplings between the junction mode and the cavity mode. Furthermore, $\tilde{\omega}_a$ and $\tilde{\omega}_b$ are given by

$$\begin{aligned}\tilde{\omega}_a &= \omega_a - \chi_{aa} - \frac{\chi_{ab}}{2} - \chi_{ab} \sum_{k=1}^{3} |\xi_k|^2 \\ \tilde{\omega}_b &= \omega_b - \chi_{bb} - \frac{\chi_{ab}}{2} - 2\chi_{bb} \sum_{k=1}^{3} |\xi_k|^2.\end{aligned}$$

Finally, the two-photon exchange strengths g_k are given by

$$g_{1/2} = -\frac{\chi_{ab}}{2} \xi_{1/2} \quad \text{and} \quad g_3 = \frac{\chi_{bb}}{2} \xi_3^{*2}.$$

Going into rotating frame with respect to $H_0/\hbar = \tilde{\omega}_a \hat{a}^\dagger \hat{a} + (\tilde{\omega}_b - \delta) \hat{b}^\dagger \hat{b} - \frac{\chi_{bb}}{2} \hat{b}^{\dagger 2} \hat{b}^2$, the Hamiltonian becomes

$$\begin{aligned}\frac{H_{\text{I}}(t)}{\hbar} = {} & \delta \hat{b}^\dagger \hat{b} - \frac{\chi_{aa}}{2} \hat{a}^{\dagger 2} \hat{a}^2 - \chi_{ab} \hat{a}^\dagger \hat{a} \hat{b}^\dagger \hat{b} + (g_1 \exp[i(\chi_{bb} \hat{b}^\dagger \hat{b} + \Delta)t] \hat{a}^{\dagger 2} \hat{b} + \text{h.c.}) \\ & + (g_2 \exp[i(\chi_{bb}(\hat{b}^\dagger \hat{b} - 1) - \Delta)t] \hat{a}^{\dagger 2} \hat{b} + \text{h.c.}) - (g_3 \exp[2i\chi_{bb} \hat{b}^\dagger \hat{b}] \hat{b}^2 + \text{h.c.})\end{aligned}$$

As outlined in [32], we perform second-order RWA to get

$$H_{\text{eff}} = \overline{H_{\text{I}}(t)} - i\overline{(H_{\text{I}}(t) - \overline{H_{\text{I}}(t)}) \int \text{d}t (H_{\text{I}}(t) - \overline{H_{\text{I}}(t)})}$$

where $\overline{A(t)} = \lim_{T\to\infty} \frac{1}{T} \int_0^T A(t)\text{d}t$. Using the expression for $H_{\text{I}}(t)$, we get

$$\begin{aligned}\frac{H_{\text{eff}}}{\hbar} = {} & ((g_{4\text{ph}} \hat{a}^{\dagger 4} - \epsilon_{4\text{ph}}) \hat{\sigma}_{fg} + \text{h.c.}) + \left(\zeta_{gaa} \hat{\sigma}_{gg} + \zeta_{eaa} \hat{\sigma}_{ee} + \zeta_{faa} \hat{\sigma}_{ff} - \frac{\chi_{aa}}{2}\right) \hat{a}^{\dagger 2} \hat{a}^2 \\ & + ((\chi_{ea} - \chi_{ab}) \hat{\sigma}_{ee} + (\chi_{fa} - 2\chi_{ab}) \hat{\sigma}_{ff}) \hat{a}^\dagger \hat{a} + \left(\delta + \frac{\chi_{ea}}{2} - \frac{3|g_3|^2}{\chi_{bb}}\right) \hat{\sigma}_{ee} + \left(2\delta + \frac{\chi_{fa}}{2}\right) \hat{\sigma}_{ff}\end{aligned} \tag{3}$$

where we have only considered the first three energy levels g, e and f of the junction mode. The other energy levels of this mode are not populated in this scheme. The transition operators $\hat{\sigma}_{jk}$ are given by $|k\rangle\langle j|$. The first two terms of equation (3) are the four-photon exchange term and the two-photon $g \leftrightarrow f$ drive on the junction

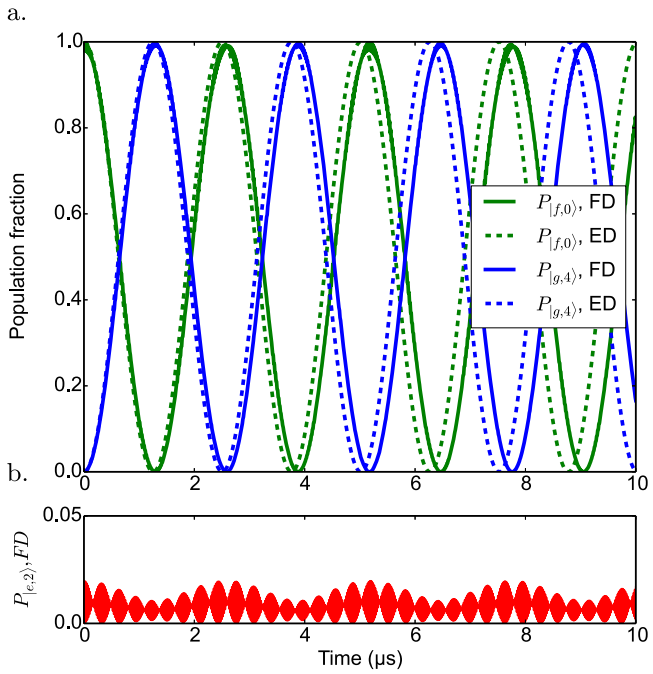

Figure 2. Numerical simulation of four-photon exchange process. (a) We compare the effective dynamics (ED) given by the Hamiltonian (3) with the full dynamics (FD) corresponding to (2). For the four-photon exchange we do not need the $g \leftrightarrow f$ Rabi drive (see text). Consequently we set $g_3 = 0$ in these equations. We start in the state $|f, 0\rangle$ and monitor the population of $|g, 4\rangle$ (blue) and $|f, 0\rangle$ (green). (b) Population leakage to the state $|e, 2\rangle$. The system parameters are $\chi_{aa}/(2\pi) = 312$ Hz, $\chi_{bb}/(2\pi) = 200$ MHz, $\chi_{ab}/(2\pi) = 0.5$ MHz. We choose $\delta = 153$ kHz, $\Delta = 50$ MHz, $g_1/(2\pi) = 899$ kHz, $g_2/(2\pi) = 2$ MHz in order to satisfy (4).

mode with

$$g_{4\mathrm{ph}} = \sqrt{2} g_1 g_2 \left(\frac{1}{\Delta} - \frac{1}{\chi_{bb} + \Delta} \right) \text{and } \epsilon_{4\mathrm{ph}} = \sqrt{2} g_3.$$

In addition to this, the pumping also modifies the cross-Kerr terms by

$$\chi_{ea} = \frac{4|g_2|^2}{\chi_{bb} - \Delta} - \frac{4|g_1|^2}{\Delta},$$
$$\chi_{fa} = \frac{8|g_2|^2}{\Delta} - \frac{8|g_1|^2}{\chi_{bb} + \Delta}$$

and produces higher-order interactions

$$\zeta_{gaa} = \left(\frac{|g_1|^2}{\Delta} - \frac{|g_2|^2}{\chi_{bb} + \Delta} \right),$$
$$\zeta_{eaa} = \left(- \frac{|g_1|^2 (\chi_{bb} - \Delta)}{\Delta(\chi_{bb} + \Delta)} - \frac{|g_2|^2 (2\chi_{bb} + \Delta}{\Delta(\chi_{bb} + \Delta)} \right),$$
$$\zeta_{faa} = \left(\frac{|g_2|^2 (2\chi_{bb} + \Delta)}{\Delta(\chi_{bb} - \Delta)} - \frac{|g_1|^2}{2\chi_{bb} + \Delta} \right).$$

To show the correctness of the effective dynamics, let us consider the oscillations between the states $|f, 0\rangle$ and $|g, 4\rangle$. Note that the population of the state $|e, n-2\rangle$ will remain small. The terms $(\zeta_{gaa}\hat{\sigma}_{gg} - \chi_{aa}/2)\hat{a}^{\dagger 2}\hat{a}^2$ and $(2\delta + \chi_{fa}/2)\hat{\sigma}_{ff}$ produce additional frequency shifts between $|g, 4\rangle$ and $|f, 0\rangle$, thus hindering the oscillations. We counter the effect of these terms by selecting parameters such that

$$\zeta_{gaa} = \frac{\chi_{aa}}{2} \text{ and } \delta = -\frac{\chi_{fa}}{4}. \tag{4}$$

The dynamics given by Hamiltonian in (2) (simulated in the rotating frame of $\tilde{\omega}_a \hat{a}^\dagger \hat{a} + \tilde{\omega}_b \hat{b}^\dagger \hat{b}$) is compared with the effective dynamics given by Hamiltonian (3) in figure 2(a). The system parameters are $\chi_{aa}/(2\pi) = 312$ Hz, $\chi_{bb}/(2\pi) = 200$ MHz, $\chi_{ab}/(2\pi) = 0.5$ MHz satisfying $\chi_{ab} = 2\sqrt{\chi_{aa}\chi_{bb}}$ [31]. The values $\Delta/(2\pi) = 50$ MHz, $\delta = 153$ kHz, $g_1/(2\pi) = 899$ kHz and $g_2/(2\pi) = 2$ MHz are selected to satisfy (4). The third drive g_3 is set to zero in this simulation. Dynamics given by both, equations (2) and (3), show the required

oscillations. The slight mismatch between the oscillation frequencies is due to a higher-order effect induced by the occupation of the state $|e,\ 2\rangle$. Figure 2(b) shows the population leakage to the $|e,\ 2\rangle$ state. This leakage leads to an important limitation of the protocol (see section 3.1).

3. Four-photon driven-dissipative process

In the last section, we showed that we get a four-photon exchange Hamiltonian (3) by cascading two-photon exchange processes. In this section, we combine this idea with the dissipation of the junction mode to achieve a four-photon driven-dissipative dynamics on the cavity mode. In section 3.1, we present the effective master equation governing the dynamics of the cavity. In particular, we observe that as an undesired effect of population leakage towards the e state, we introduce a two-photon dissipation on the cavity mode. This problem is addressed in section 3.2 by engineering the noise spectral density seen by the junction mode. Additionally, we analyse the performance of the proposed schemes through numerical simulations of the full and effective master equations.

3.1. Effective master equation

We consider the junction mode to be coupled to a cold bath, leading to the master equation

$$\frac{\mathrm{d}}{\mathrm{d}t}\rho = -\frac{i}{\hbar}[H_{\mathrm{sys}}(t),\ \rho] + \Gamma_1\mathcal{D}[\hat{b}]\rho. \tag{5}$$

where the Hamiltonian H_{sys} is given by (2). Note that this master equation implicitly assumes a white-noise spectrum for the bath degrees of freedom. In appendix A, we will provide a more general analysis considering an arbitrary noise spectrum. Indeed, in this appendix, we perform RWA under such general assumptions, arriving at a time-independent master equation for the junction-cavity system. Under the assumption of strong dissipation, we can also eliminate the junction degrees of freedom, resulting in an effective master equation for the cavity mode (see appendix B):

$$\frac{\mathrm{d}}{\mathrm{d}t}\rho_{\mathrm{cav}} = -i[(\zeta_{gaa} - \chi_{aa})\hat{a}^{\dagger 2}\hat{a}^2,\ \rho_{\mathrm{cav}}] + \kappa_{4\mathrm{ph}}\mathcal{D}[\hat{a}^4 - \alpha^4]\rho_{\mathrm{cav}} + \kappa_{2\mathrm{ph}}\mathcal{D}[\hat{a}^2]\rho_{\mathrm{cav}} \tag{6}$$

with

$$\begin{aligned}\kappa_{4\mathrm{ph}} &= \frac{2|g_{4\mathrm{ph}}|^2}{\Gamma_1},\\ \kappa_{2\mathrm{ph}} &= \left(\frac{|g_1|^2}{\Delta^2} + \frac{|g_2|^2}{(\Delta + \chi_{bb})^2}\right)\Gamma_1,\\ \alpha &= \left(\frac{\epsilon_{4\mathrm{ph}}}{g_{4\mathrm{ph}}}\right)^{1/4}.\end{aligned} \tag{7}$$

While we get the expected four-photon driven-dissipative term $\kappa_{4\mathrm{ph}}\mathcal{D}[\hat{a}^4 - \alpha^4]$, we also inherit an undesired two-photon dissipation $\kappa_{2\mathrm{ph}}\mathcal{D}[\hat{a}^2]$. Such a two-photon dissipation corresponds to jumps between states with same photon-number parities thus effectively introducing bit-flip errors in the logical code space [24]. In the next subsection, we will remedy this problem by engineering the dissipation of the junction mode.

To establish the validity of equation (6), we numerically compare the dynamics of the two master equations (5) and (6). The blue curves in figures 3(a) and (b) correspond to these simulations. We initialise the system in its ground state and plot the overlap with the cat state $|\mathcal{C}_\alpha^{(0\bmod 4)}\rangle = \mathcal{N}(|\alpha\rangle + |-\alpha\rangle + |i\alpha\rangle + |-i\alpha\rangle)$ where $\mathcal{N}$ is a normalisation factor. Note that as the cavity is initialised in the vacuum state, we expect the four-photon driven-dissipative process to steer the state towards $|\mathcal{C}_\alpha^{(0\bmod 4)}\rangle$ [24]. The chosen system parameters are the same as in the last section. The additional dissipation parameter $\Gamma_1/(2\pi) = 2$ MHz. We also select $g_3/(2\pi) = 460$ kHz to achieve a cat amplitude of $\alpha = 2$. These parameters give $1/\kappa_{4\mathrm{ph}} \sim 96\ \mu$s and $1/\kappa_{2\mathrm{ph}} = 205\ \mu$s. The maximum achieved overlap with the target state ($|\mathcal{C}_\alpha^{(0\bmod 4)}\rangle$) is merely above 50%. This is expected, as the two-photon dissipation rate is not much smaller than the four-photon dissipation rate. More precisely, the resulting steady state is a mixture of two even parity states represented by the Wigner function in figure 3(c). Note that while this is a mixed state, the conservation of the photon-number parity leads to negative values in the Wigner function.

3.2. Mitigation of two-photon dissipation error

As mentioned in the previous subsection, the inherited two-photon dissipation can be seen as a bit-flip error channel in the code space. Its rate has to be compared with the rate of other errors that are not corrected by the four-component cat code. Indeed, this code can only correct for a single-photon loss in the time interval δt

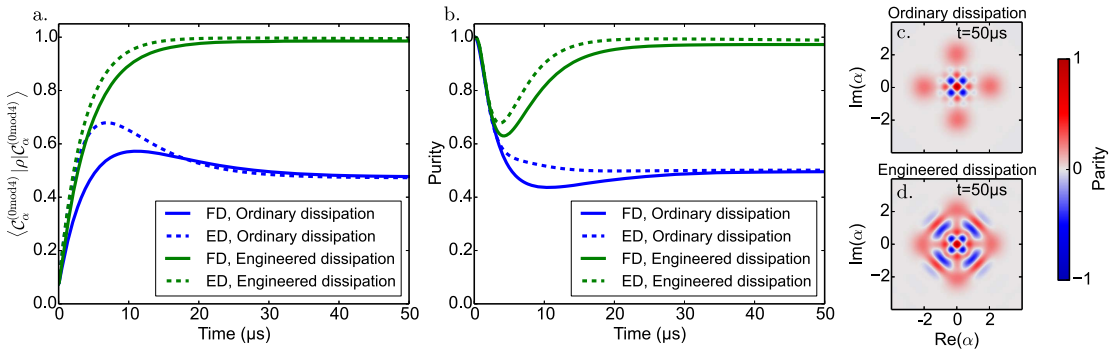

Figure 3. Simulation results for the full dynamics (FD, solid lines) given by the master equation (9) and for the effective master equation (6) (ED, dashed lines) with κ_{4ph} and κ_{2ph} given by (8) and (7) respectively. The blue curves correspond to a white-noise spectrum (ordinary dissipation) described in section 3.1 and the green curves illustrate the result for an engineered f to g dissipation as in section 3.2. Panel (a) presents the overlap of the density matrix with the state $|\mathcal{C}_\alpha^{(0\,\mathrm{mod}\,4)}\rangle$ and panel (b) plots the purity of the cavity state. Panel (c) and panel (d) show the Wigner functions at $t = 50\ \mu$s. The superior performance of the engineered dissipation is apparent from the results. The simulation parameters are $\chi_{bb}/(2\pi) = 200$ MHz, $\chi_{aa}/(2\pi) = 312$ Hz, $\chi_{ab}/(2\pi) = 0.5$ MHz, $\Delta/(2\pi) = 50$ MHz, $g_2/(2\pi) = 2$ MHz and $g_1/(2\pi) = 899$ kHz such that $\zeta_{gaa} = \chi_{aa}/2$. For the ordinary dissipation $\Gamma_1/(2\pi) = 2$ MHz, and for the engineered dissipation $\Gamma_1/(2\pi) = 3$ kHz with the $f \to g$ direct dissipation given by $\Gamma_{fg}^{\mathrm{eng}}/(2\pi) = 4$ MHz.

between two error syndrome (photon-number parity) measurements. The probability of two single-photon losses during δt is given by $p_1^{2\mathrm{ph}} = (|\alpha|^2\kappa_{1ph}\delta t)^2/2$. Whereas the probability for a direct two-photon loss due to the $\hat{a}^2$ dissipation is $p_2^{2\mathrm{ph}} = |\alpha|^4\kappa_{2\mathrm{ph}}\delta t$. Hence, we require the induced error probability $p_2^{2\mathrm{ph}}$ to be of the same order or smaller than $p_1^{2\mathrm{ph}}$. Therefore, we need to reduce $\kappa_{2\mathrm{ph}}$ to a value smaller than $\kappa_{1\mathrm{ph}}^2\delta t/2$. In this subsection, we propose a simple modification of the above scheme, which, with currently achievable experimental parameters, should lead to $\kappa_{2\mathrm{ph}}/\kappa_{1\mathrm{ph}}$ to be less than 0.01.

One such approach is to use a dynamically engineered coupling of the junction mode to the bath. More precisely, we start with a high-Q junction mode corresponding to a small Γ_1 with respect to the Hamiltonian parameters. By dispersively coupling this mode to a low-Q resonator in the photon-number resolved regime [33], one can engineer a dynamical cooling protocol similar to DDROP [34], or parametric sideband cooling [35, 36]. While these experiments correspond to a dynamical cooling from e to g, one can easily modify them to achieve a direct dissipation from f to g. Here, we model this engineered dissipation by adding a Lindblad term of the form $\Gamma_{fg}^{\mathrm{eng}}\mathcal{D}[\hat{\sigma}_{fg}]\rho$. This leads to the new dissipation rate

$$\kappa_{4\mathrm{ph}} = \frac{4|g_{4\mathrm{ph}}|^2}{\Gamma_{fg}^{\mathrm{eng}} + 2\Gamma_1}, \tag{8}$$

while the two-photon dissipation rate $\kappa_{2\mathrm{ph}}$ remains unchanged, as given by (7).

The green curves in figures 3(a) and (b) illustrate the numerical simulations of this modified scheme. The solid curves correspond to the simulation of the master equation

$$\frac{\mathrm{d}}{\mathrm{d}t}\rho = -\frac{i}{\hbar}[H_{\mathrm{sys}}(t),\ \rho] + \Gamma_1\mathcal{D}[\hat{b}]\rho + \Gamma_{fg}^{\mathrm{eng}}\mathcal{D}[\hat{\sigma}_{fg}]\rho, \tag{9}$$

with $\Gamma_1/(2\pi) = 3$ kHz and $\Gamma_{fg}^{\mathrm{eng}}/(2\pi) = 4$ MHz. This value is a compromise between the strength of $\kappa_{4\mathrm{ph}}$ and the validity of the adiabatic elimination, as shown in appendix B. Similarly, the dashed green curves correspond to the simulation of (6) with $\kappa_{4\mathrm{ph}}$ now given by (8). Indeed, with these parameters, we achieve $1/\kappa_{4\mathrm{ph}} \sim 96\ \mu$s and $1/\kappa_{2\mathrm{ph}} = 136$ ms. In appendix B, we will provide an alternative approach based on using band-pass Purcell filters [37], shaping the noise spectrum seen by the junction mode.

4. Conclusion

We have presented a theoretical proposal for the implementation of a controlled four-photon driven-dissipative process on a harmonic oscillator. By stabilising the manifold span $\{|\pm\alpha\rangle, |\pm i\alpha\rangle\}$, this process provides a means to realise an error-corrected logical qubit [24]. Our proposal relies on cascading two-photon exchange processes, which have already been experimentally demonstrated [25]. While the required hardware complexity is similar to the existing system, the parameters need to be carefully chosen to avoid undesired interactions.

The technique of cascading nonlinear processes through Raman-like virtual transitions can be used to engineer other highly nonlinear interactions. In particular, a Hamiltonian of the form $g_{12}\hat{a}_1^{2\dagger}\hat{a}_2^2 + g_{12}^*\hat{a}_1^2\hat{a}_2^{2\dagger}$ could entangle two logical qubits encoded in two high-Q cavities $\hat{a}_1$ and $\hat{a}_2$ [24]. Such an interaction can be

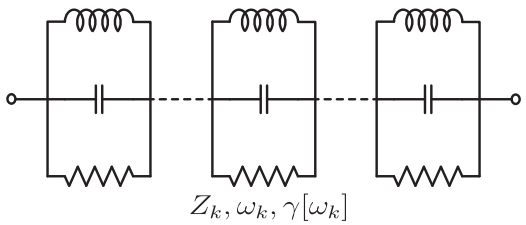

Figure 4. Modelling dissipation using LCR elements [38]. The system is assumed to be linearly coupled to infinitely many dissipative harmonic oscillators with finite frequency spacing. This can be seen as a discretisation of a general noise spectrum using a basis of Lorentzian functions.

generated by coupling the cavities through a Josephson junction mode $\hat{b}$ and applying two off-resonant pumps at frequencies $\omega_{p1} = 2\tilde{\omega}_{a1} - \tilde{\omega}_b - \Delta$ and $\omega_{p2} = 2\tilde{\omega}_{a2} - \tilde{\omega}_b - \Delta$. This entangling gate constitutes another important step towards fault-tolerant universal quantum computation with cat-qubits.

Acknowledgements

We acknowledge fruitful discussions with Ananda Roy, Zlatko Minev and Richard Brierly. This research was supported by INRIAs DPEI under the TAQUILLA associated team and by ARO under Grant No. W911NF-14-1-0011.

Appendix A. RWA in presence of dissipation

We start by considering the Hamiltonian of a junction-cavity system where the junction mode is dissipative. This dissipation is typically modelled by a linear coupling to a continuum of infinitely many non-dissipative modes [39]. Here, we instead model this dissipation by a linear coupling of the junction mode to infinitely many harmonic oscillators with finite frequency spacing and finite bandwidths. Indeed, for an under-coupled system (weak dissipation), we can use LCR elements [31, 38] to represent the dissipation in terms of such dissipative oscillators (see figure 4). Such a discretisation could also be explained taking into account experimental considerations where the dissipation is mediated by various filters which could themselves be seen as lossy resonators. More precisely, we consider a Hamiltonian

$$\frac{H_{\rm tot}}{\hbar} = \frac{H_{\rm sys}}{\hbar} + \sum_k \omega_k \hat{c}^\dagger[\omega_k]\hat{c}[\omega_k] + \sum_k (\Omega[\omega_k]\hat{b}\hat{c}^\dagger[\omega_k] + \Omega^*[\omega_k]\hat{b}^\dagger\hat{c}[\omega_k]),$$

where $H_{\rm sys}$ is the system Hamiltonian given in (2) and the modes $\hat{c}[\omega_k]$ have decay rates $\gamma[\omega_k]$. We perform the second-order RWA on the associated master equation by going into the rotating frame of $\widetilde{H}_0 = \tilde{\omega}_a\hat{a}^\dagger\hat{a} + \tilde{\omega}_b\hat{b}^\dagger\hat{b} - \frac{\chi_{bb}}{2}\hat{b}^{\dagger 2}\hat{b}^2 + \sum_k \hbar\omega_k\hat{c}^\dagger[\omega_k]\hat{c}[\omega_k]$. The effective master equation becomes

$$\begin{aligned}\frac{\mathrm{d}}{\mathrm{d}t}\rho = &-\frac{i}{\hbar}[H_{\rm eff,bath},\,\rho] + \sum_k (1 + n_{\rm th}[\omega_k])\gamma[\omega_k]\mathcal{D}[\hat{c}[\omega_k]]\rho \\ &+ \sum_k n_{\rm th}[\omega_k]\gamma[\omega_k]\mathcal{D}[\hat{c}^\dagger[\omega_k]]\rho\end{aligned}$$

where $n_{\rm th}[\omega_k]$ implies the thermal population of the kth mode. The Hamiltonian $H_{\rm eff,bath}$ is given by

$$\begin{aligned}\frac{H_{\rm eff,bath}}{\hbar} \approx \frac{H_{\rm eff}}{\hbar} &+ \sum_{n=0}^{\infty}(\Omega[\tilde{\omega}_b - (n-1)\chi_{bb}]\hat{c}^\dagger[\tilde{\omega}_b - \chi_{bb}]\sqrt{n}\,\hat{\sigma}_{n,n-1} + \text{h.c.}) \\ &+ (g_1^*\Omega[\omega_{+\Delta,0}]\hat{c}^\dagger[\omega_{+\Delta,0}]\hat{a}^2 + \text{h.c.})\sum_{n=0}^{\infty}\frac{\chi_{bb} - \Delta}{(n\chi_{bb} + \Delta)((n-1)\chi_{bb} + \Delta)}\hat{\sigma}_{n,n} \\ &+ (g_2^*\Omega[\omega_{-\Delta,1}]\hat{c}^\dagger[\omega_{-\Delta,1}]\hat{a}^2 + \text{h.c.})\sum_{n=0}^{\infty}\frac{2\chi_{bb} + \Delta}{((n-2)\chi_{bb} - \Delta)((n-1)\chi_{bb} - \Delta)}\hat{\sigma}_{n,n} \\ &+ \sum_{n=0}^{\infty}\left(\frac{g_1\chi_{bb}\Omega[\omega_{+\Delta,2n}]}{(n\chi_{bb} + \Delta)((n+1)\chi_{bb} + \Delta)}\hat{c}^\dagger[\omega_{+\Delta,2n}]\hat{a}^{\dagger 2}\sqrt{(n+1)(n+2)}\,\hat{\sigma}_{n+2,n} + \text{h.c.}\right) \\ &+ \sum_{n=0}^{\infty}\left(\frac{g_2\chi_{bb}\Omega[\omega_{-\Delta,2n+1}]}{(n\chi_{bb} - \Delta)((n-1)\chi_{bb} - \Delta)}\hat{c}^\dagger[\omega_{-\Delta,2n+1}]\hat{a}^{\dagger 2}\sqrt{(n+1)(n+2)}\,\hat{\sigma}_{n+2,n} + \text{h.c.}\right). \qquad \text{(A1)}\end{aligned}$$

Here, n indicates the number states of the junction mode (specifically $n = 0, 1, 2$ correspond to g, e, f levels in the main text). The frequencies $\omega_{\pm\Delta,n}$ are defined as $\tilde{\omega}_b \pm \Delta - n\chi_{bb}$. Along with the terms presented in (A1), we also obtain terms of the form $\hat{\sigma}_{nn}\hat{c}^\dagger[\omega_k]\hat{c}[\omega_k]$ and $\hat{\sigma}_{n+2,n}\hat{c}^\dagger[\omega_k]\hat{c}^\dagger[\omega_m] + \text{h.c.}$ The first type of terms corresponds to the dispersive coupling of the junction mode and the bath modes. For non-zero bath temperature, they contribute to the dephasing of the junction mode states. The latter terms become resonant when $\hbar(\omega_k + \omega_m)$ equals the energy difference between the states n and $n+2$ of the junction mode and give rise to a direct two-photon dissipation between the two states. As stated in section 3.2 such a direct dissipation from the f to g state actually enhances the performance of the protocol. However, without additional engineering, the magnitude of such interactions is negligible compared to the regular single-photon dissipation terms in (A1).

Next, by adiabatically eliminating the highly dissipative bath modes, we obtain the master equation

$$\begin{aligned}\frac{\mathrm{d}}{\mathrm{d}t}\rho = &-\frac{i}{\hbar}[H_{\text{eff}},\rho] + \sum_{n=0}^{\infty}(n\Gamma_\downarrow[\tilde{\omega}_b-(n-1)\chi_{bb}]\mathcal{D}[\hat{\sigma}_{n,n-1}] + n\Gamma_\uparrow[\tilde{\omega}_b-(n-1)\chi_{bb}]\mathcal{D}[\hat{\sigma}_{n-1,n}])\rho\\
&+\sum_{n=0}^{\infty}\left(\frac{|g_1|(\chi_{bb}-\Delta)}{(n\chi_{bb}+\Delta)((n-1)\chi_{bb}+\Delta)}\right)^2(\Gamma_\downarrow[\omega_{+\Delta,0}]\mathcal{D}[\hat{a}^2\hat{\sigma}_{n,n}] + \Gamma_\uparrow[\omega_{+\Delta,0}]\mathcal{D}[\hat{a}^{\dagger 2}\hat{\sigma}_{n,n}])\rho\\
&+\sum_{n=0}^{\infty}\left(\frac{|g_2|(2\chi_{bb}+\Delta)}{((n-2)\chi_{bb}-\Delta)((n-1)\chi_{bb}-\Delta)}\right)^2(\Gamma_\downarrow[\omega_{-\Delta,1}]\mathcal{D}[\hat{a}^2\hat{\sigma}_{n,n}] + \Gamma_\uparrow[\omega_{-\Delta,1}]\mathcal{D}[\hat{a}^{\dagger 2}\hat{\sigma}_{n,n}])\rho\\
&+\sum_{n=0}^{\infty}\left(\frac{\sqrt{(n+1)(n+2)}\,|g_1|\chi_{bb}}{(n\chi_{bb}+\Delta)((n+1)\chi_{bb}+\Delta)}\right)^2(\Gamma_\downarrow[\omega_{+\Delta,2n}]\mathcal{D}[\hat{a}^{\dagger 2}\hat{\sigma}_{n+2,n}] + \Gamma_\uparrow[\omega_{+\Delta,2n}]\mathcal{D}[\hat{a}^2\hat{\sigma}_{n,n+2}])\rho\\
&+\sum_{n=0}^{\infty}\left(\frac{\sqrt{(n+1)(n+2)}\,|g_2|\chi_{bb}}{(n\chi_{bb}-\Delta)((n-1)\chi_{bb}-\Delta)}\right)^2(\Gamma_\downarrow[\omega_{-\Delta,2n+1}]\mathcal{D}[\hat{a}^{\dagger 2}\hat{\sigma}_{n+2,n}] + \Gamma_\uparrow[\omega_{-\Delta,2n+1}]\mathcal{D}[\hat{a}^2\hat{\sigma}_{n,n+2}])\rho\end{aligned} \tag{A2}$$

where

$$\Gamma_\downarrow[\omega] = \frac{4(1+n_{\text{th}}[\omega])|\Omega[\omega]|^2}{\gamma[\omega]}$$
$$\Gamma_\uparrow[\omega] = \frac{4n_{\text{th}}[\omega]|\Omega[\omega]|^2}{\gamma[\omega]}.$$

In the next section, we study the adiabatic elimination of the junction mode.

Appendix B. Validity of adiabatic elimination

Here, we limit ourselves to the lowest three levels ($|g\rangle$, $|e\rangle$ and $|f\rangle$) of the junction mode and furthermore we assume the bath to be at zero temperature. Additionally, following the discussion in section 3.2, we consider the case of an engineered bath potentially leading to a strong direct dissipation from f to g. The master equation is given by

$$\begin{aligned}\frac{\mathrm{d}}{\mathrm{d}t}\rho = &-\frac{i}{\hbar}[H_{\text{eff}},\rho] + (\Gamma_\downarrow[\tilde{\omega}_b]\mathcal{D}[\hat{\sigma}_{eg}] + 2\Gamma_\downarrow[\tilde{\omega}_b-\chi_{bb}]\mathcal{D}[\hat{\sigma}_{fe}])\rho + (\kappa_{2,gg}\mathcal{D}[\hat{a}^2\hat{\sigma}_{gg}] + \kappa_{2,ee}\mathcal{D}[\hat{a}^2\hat{\sigma}_{ee}]\\
&+\kappa_{2,ff}\mathcal{D}[\hat{a}^2\hat{\sigma}_{ff}])\rho + \Gamma_{fg}^{\text{eng}}\mathcal{D}[\hat{\sigma}_{fg}]\rho + \kappa_{2,fg}\mathcal{D}[\hat{a}^{\dagger 2}\hat{\sigma}_{fg}]\rho\end{aligned} \tag{B1}$$

where the decay rates $\kappa_{2,gg}$, $\kappa_{2,ee}$, $\kappa_{2,ff}$ and $\kappa_{2,fg}$ can be inferred from (A2). The rate Γ_{fg}^{eng} corresponds to the engineered direct dissipation from f to g. Assuming $2\Gamma_\downarrow[\tilde{\omega}_b-\chi_{bb}] + \Gamma_{fg}^{\text{eng}} \gg \|H_{\text{eff}}/\hbar\|$, we adiabatically eliminate the junction mode to obtain the master equation in (6). Note, however, that for this general noise spectrum, the effective dissipation rates are given by

$$\kappa_{4\text{ph}} = \frac{4|g_{4\text{ph}}|^2}{2\Gamma_\downarrow[\tilde{\omega}_b-\chi_{bb}] + \Gamma_{fg}^{\text{eng}}},$$
$$\kappa_{2\text{ph}} = \frac{|g_1|^2}{\Delta^2}\Gamma_\downarrow[\tilde{\omega}_b+\Delta] + \frac{|g_2|^2}{(\Delta+\chi_{bb})^2}\Gamma_\downarrow[\tilde{\omega}_b-\Delta-\chi_{bb}]. \tag{B2}$$

The rates given in (7) and (8) correspond to the white-noise case where $\Gamma_\downarrow[\omega_k] = \Gamma_1$ for all k.

The above general result provides another possible approach to mitigate the problem of the undesired two-photon dissipation. The two dissipation rates $\kappa_{4\text{ph}}$ and $\kappa_{2\text{ph}}$ from (B2) are sensitive to noise at different frequencies. While $\kappa_{4\text{ph}}$ involves the noise at frequency $\tilde{\omega}_b - \chi_{bb}$, the undesired $\kappa_{2\text{ph}}$ involves the noise at frequencies $\omega_1 = \tilde{\omega}_b + \Delta$ and $\omega_2 = \tilde{\omega}_b - \Delta - \chi_{bb}$. It is possible to engineer the coupling of the system to an

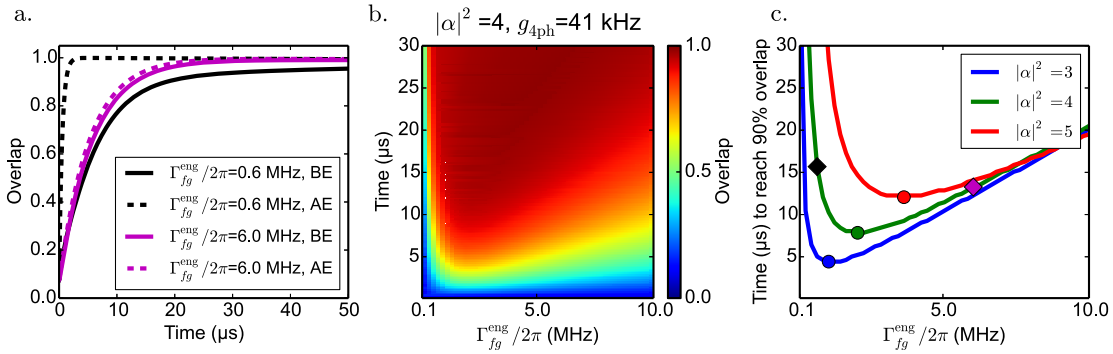

Figure 5. Panel (a) compares the system dynamics before (B1) and after (6) the adiabatic elimination, denoted respectively by (BE) and (AE). We use the same parameters as in figure 3 together with $\Gamma_{fg}^{eng}/2\pi = 0.6$ MHz (black) and $\Gamma_{fg}^{eng}/2\pi = 6$ MHz (magenta). We initialise the system in the ground state and plot the overlap $\langle \mathcal{C}_\alpha^{(0 \bmod 4)} | \rho | \mathcal{C}_\alpha^{(0 \bmod 4)} \rangle$. Panel (b) shows the overlap as a function of time, obtained by simulating (B1) with $\Gamma_{fg}^{eng}/2\pi$ ranging from 0.1 MHz to 10 MHz. Panel (c) plots the time taken to achieve 90% fidelity as a function of Γ_{fg}^{eng} for $|\alpha|^2 = 3$, 4 and 5. Black and magenta squares indicate the choices $\Gamma_{fg}^{eng}/2\pi = 0.6$ MHz and $\Gamma_{fg}^{eng}/2\pi = 6$ MHz, corresponding to the simulations of (a). The dots correspond to the optimum working points for various cat amplitudes.

electromagnetic bath such that $\Gamma_\downarrow[\tilde{\omega}_b]$, $\Gamma_\downarrow[\tilde{\omega}_b - \chi_{bb}] \gg \Gamma_\downarrow[\omega_1]$, $\gamma_\downarrow[\omega_2]$. Indeed, one can mediate the coupling between the system and the bath through a band-pass filter. This is a more elaborate version of the Purcell filter realised in [37]. The frequencies $\tilde{\omega}_b$ and $\tilde{\omega}_b - \chi_{bb}$ have to be in the pass band, whereas the frequencies ω_1 and ω_2 have to be in the cut-off.

The rest of this appendix is devoted to checking the validity of this adiabatic elimination through numerical simulations. In figure 5(a), we compare the dynamics given by (B1) and (6), using the same parameters as in figure 3 (corresponding to $|\alpha|^2 = 4$ and $g_{4ph}/2\pi = 41$ kHz), and taking $\Gamma_{fg}^{eng}/2\pi = 0.6$ MHz (black) and $\Gamma_{fg}^{eng}/2\pi = 6$ MHz (magenta). For the considered amplitude $|\alpha|^2 = 4$, the choice of $\Gamma_{fg}^{eng}/2\pi = 6$ MHz satisfies the above separation of time-scales, leading to a good agreement between the dashed and solid magenta lines. The choice of $\Gamma_{fg}^{eng}/2\pi = 0.6$ MHz leads to a disagreement with the reduced dynamics. Note that the dynamics still converges towards the expected state albeit at a slower rate. To choose the optimum working point, we perform simulations of (B1), sweeping $\Gamma_{fg}^{eng}/2\pi$ from 0.1 MHz to 10 MHz. In figure 5(b) we plot the overlap with the $|\mathcal{C}_\alpha^{(0 \bmod 4)}\rangle$ cat state as a function of time and Γ_{fg}^{eng}. From this, we extract the time taken to achieve 90% fidelity as a function of Γ_{fg}^{eng}. This corresponds to the green curve in figure 5(c). As illustrated by the green dot, the optimum working point is given by $\Gamma_{fg}^{eng}/2\pi = 2$ MHz. Note that the working point of $\Gamma_{fg} = 4$ MHz used in figure 3 is selected to be well in the region of adiabatic validity while still getting a strong four-photon dissipation (κ_{4ph}). The same simulations for $|\alpha|^2 = 3$ and 5 give rise to different working points at 1 MHz and 3.7 MHz respectively. Indeed, the norm $\|H_{eff}\|$, in the assumption $2\Gamma_\downarrow[\tilde{\omega}_b - \chi_{bb}] + \Gamma_{fg}^{eng} \gg \|H_{eff}/\hbar\|$, corresponds to the norm of the Hamiltonian when confined to the code space span $\{|\pm\alpha\rangle, |\pm i\alpha\rangle\}$. This implies a separation of time-scales which depends on the amplitude $|\alpha|$ of the cat state, therefore leading to different optimum working points.

References

[1] Zanardi P and Rasetti M 1997 *Phys. Rev. Lett.* **79** 3306
[2] Lidar D A, Chuang I L and Whaley K B 1998 *Phys. Rev. Lett.* **81** 2594
[3] Kempe J, Bacon D, Lidar D A and Whaley K B 2001 *Phys. Rev.* A **63** 042307
[4] Knill E, Laflamme R and Viola L 2000 *Phys. Rev. Lett.* **84** 2525
[5] Albert V V, Bradlyn B, Fraas M and Jiang L 2015 arXiv: 1512.08079
[6] Poyatos J F, Cirac J I and Zoller P 1996 *Phys. Rev. Lett.* **77** 4728
[7] Plenio M B, Huelga S F, Beige A and Knight P L 1999 *Phys. Rev.* A **59** 2468
[8] Carvalho A R R, Milman P, de Matos Filho R L and Davidovich L 2001 *Phys. Rev. Lett.* **86** 4988
[9] Verstraete F, Wolf M M and Ignacio Cirac J 2009 *Nat Phys* **5** 633
[10] Sarlette A, Raimond J M, Brune M and Rouchon P 2011 *Phys. Rev. Lett.* **107** 010402
[11] Krauter H, Muschik C A, Jensen K, Wasilewski W, Petersen J M, Cirac J I and Polzik E S 2011 *Phys. Rev. Lett.* **107** 080503
[12] Kastoryano M J, Reiter F and Sørensen A S 2011 *Phys. Rev. Lett.* **106** 090502
[13] Murch K W, Vool U, Zhou D, Weber S J, Girvin S M and Siddiqi I 2012 *Phys. Rev. Lett.* **109** 183602
[14] Leghtas Z, Vool U, Shankar S, Hatridge M, Girvin S M, Devoret M H and Mirrahimi M 2013 *Phys. Rev.* A **88** 023849
[15] Shankar S, Hatridge M, Leghtas Z, Sliwa K M, Narla A, Vool U, Girvin S M, Frunzio L, Mirrahimi M and Devoret M H 2013 *Nature* **504** 419
[16] Kronwald A, Marquardt F and Clerk A A 2013 *Phys. Rev.* A **88** 063833

[17] Lin Y, Gaebler J P, Reiter F, Tan T R, Bowler R, Sorensen A S, Leibfried D and Wineland D J 2013 *Nature* **504** 415
[18] Roy A, Leghtas Z, Stone A D, Devoret M and Mirrahimi M 2015 *Phys. Rev.* A **91** 013810
[19] Holland E T *et al* 2015 *Phys. Rev. Lett.* **115** 180501
[20] Wolinsky M and Carmichael H J 1988 *Phys. Rev. Lett.* **60** 1836
[21] Gilles L, Garraway B M and Knight P L 1994 *Phys. Rev.* A **49** 2785
[22] Hach E E III and Gerry C C 1994 *Phys. Rev.* A **49** 490
[23] Cochrane P T, Milburn G J and Munro W J 1999 *Phys. Rev.* A **59** 2631
[24] Mirrahimi M, Leghtas Z, Albert V V, Touzard S, Schoelkopf R J, Jiang L and Devoret M H 2014 *New J. Phys.* **16** 045014
[25] Leghtas Z *et al* 2015 *Science* **347** 853
[26] Gardiner C and Zoller P 2015 *The Quantum World of Ultra-Cold Atoms and Light* (London: Imperial College Press)
[27] Leghtas Z, Kirchmair G, Vlastakis B, Schoelkopf R J, Devoret M H and Mirrahimi M 2013 *Phys. Rev. Lett.* **111** 120501
[28] Sun L *et al* 2014 *Nature* **511** 444
[29] Ofek N *et al* 2016 *Nature* **536** 441
[30] Albert V V, Shu C, Krastanov S, Shen C, Liu R-B, Yang Z-B, Schoelkopf R J, Mirrahimi M, Devoret M H and Jiang L 2016 *Phys. Rev. Lett.* **116** 140502
[31] Nigg S E, Paik H, Vlastakis B, Kirchmair G, Shankar S, Frunzio L, Devoret M H, Schoelkopf R J and Girvin S M 2012 *Phys. Rev. Lett.* **108** 240502
[32] Mirrahimi M and Rouchon P 2015 Modeling and control of quantum systems http://cas.ensmp.fr/~rouchon/QuantumSyst/index.html
[33] Schuster D I *et al* 2007 *Nature* **445** 515
[34] Geerlings K, Leghtas Z, Pop I M, Shankar S, Frunzio L, Schoelkopf R J, Mirrahimi M and Devoret M H 2013 *Phys. Rev. Lett.* **110** 120501
[35] Pechal M, Huthmacher L, Eichler C, Zeytinoğlu S, Abdumalikov A A, Berger S, Wallraff A and Filipp S 2014 *Phys. Rev.* X **4** 041010
[36] Narla A *et al* 2016 *Phys. Rev.* X **6** 031036
[37] Reed M D, Johnson B R, Houck A A, DiCarlo L, Chow J M, Schuster D I, Frunzio L and Schoelkopf R J 2010 *Appl. Phys. Lett.* **96** 203110
[38] Solgun F, Abraham D W and DiVincenzo D P 2014 *Phys. Rev.* B **90** 134504
[39] Caldeira A O and Leggett A J 1983 *Ann. Phys., NY* **149** 374